2019 IEEE 20th International Conference on Information Reuse and Integration for Data Science (IRI)

Analysis of Temporal Relationships between ASD and Brain Activity through EEG and Machine Learning

Yasith Jayawardana
Computer Science
Old Dominion University
Norfolk, VA 23529
yasith@cs.odu.edu

Mark Jaime
Psychology
Indiana University-Purdue University
Columbus, IN 47203
mjaime@iupuc.edu

Sampath Jayarathna
Computer Science
Old Dominion University
Norfolk, VA 23529
sampath@cs.odu.edu

***Abstract*—Autism Spectrum Disorder (ASD) is a neurodevelopmental disorder that impairs normative social cognitive and communicative function. Early diagnosis is crucial for the timely and efficacious treatment of ASD. The Autism Diagnostic Observation Schedule Second Edition (ADOS-2) is the current gold standard for diagnosing ASD. In this paper, we analyse the short-term and long-term relationships between ASD and brain activity using Electroencephalography (EEG) readings taken during the administration of ADOS-2. These readings were collected from 8 children diagnosed with ASD, and 9 low risk controls. We derive power spectrums for each electrode through frequency band decomposition and through wavelet transforms relative to a baseline, and generate two sets of training data that captures long-term and short-term trends respectively. We utilize machine learning models to predict the ASD diagnosis and the ADOS-2 scores, which provide an estimate for the presence of such trends. When evaluating short-term dependencies, we obtain a maximum of 56% accuracy of classification through linear models. Non-linear models provide a classification above 92% accuracy, and predicted ADOS-2 scores within an RMSE of 4. We use a CNN model to evaluate the long-term trends, and obtain a classification accuracy of 95%. Our findings have implications for using EEG as a non-invasive bio-marker for ASD with minimal feature manipulation and computational overhead.**

***Index Terms*—ASD, ADOS-2, EEG, Machine Learning**

I. Introduction

Autism Spectrum Disorder (ASD) is a neuro-developmental disorder characterized by impairments in social interaction and communication, as well as the presence of repetitive behaviors and/or restricted interests. The symptoms of ASD can be broad and range in severity. ASD is neither caused by nor reducible to any single genetic, environmental, or neurocognitive factor [1], [2]. Conceptions on the origins of ASD posit that its emergence begins during the prenatal period, with the aberrant functional organization of experience-dependent neural systems that support social information processing. According to CDC estimates [3], the prevalence of ASD has nearly doubled over the last decade, with a costly impact on the families affected. It is estimated that 1 in 6 children in the US suffer from developmental disorders, with 1 in 68 children suffering from ASD. The total lifetime cost of care for an individual with ASD could be as high as $ 2.4 million [4]. In the U.S., the long-term societal costs are projected to reach $ 461 billion by 2025. Efforts to identify etiologically meaningful markers of ASD are thus critical for mitigating these costs through improvement in early diagnosis and treatment of ASD.

Current gold-standard diagnostic measures of ASD, such as the Autism Diagnostic Observation Schedule Second Edition (ADOS-2) [5], have shown significant progress in increasing the accuracy of ASD diagnosis. However, correctly administering ADOS-2 requires extensive and costly training to make accurate behavioral assessments and careful observations of often subtle social cues and overtures occurring within a limited period of time. Currently, the youngest age at which a child can be administered the ADOS-2 is 1.5 years. Nonetheless, there is a critical need for more feasible approaches that can detect ASD as early as possible, such as during infancy. This presents a unique challenge for identifying infant markers of ASD that are aligned with currently recognized social processing dimensions of ASD.

One approach is to develop low-cost, feasible, and objective measurement systems that are based on neuro-physiological data that map onto the core deficits that are represented in current diagnostic criteria. Such measures would reduce the intense labor and high cost of current diagnostic approaches as well as minimize the potential for misdiagnosis due to subjectivity and complexities in the process. One potential neuro-physiological instrument for this purpose is electroencephalography (EEG). Its high temporal resolution and ability to be applied within ecologically valid social contexts via wireless solutions allows for the acquisition of data during live social interaction [6], [7]. This makes EEG an ideal choice for examining relevant neuro-physiological features of ASD in real-world settings. Despite these advantages, the majority of EEG research on ASD has occurred in highly controlled experimental environments, requiring data collected over a large number of trials with minimal head movement.

In this paper, we analyse the temporal relationship between ASD and brain activity through neural system activity infor-

978-1-7281-1337-1/19/$31.00 ©2019 IEEE
DOI 10.1109/IRI.2019.00035

mation obtained via EEG during the administration of ADOS-2. We utilize frequency-time power metrics obtained through pre-processing of EEG data to analyse the presence short-term and long-term trends between ASD and brain activity. We train several machine learning models for diagnosing ASD and predicting ADOS-2 scores, and adopt multiple feature extraction methods to generalize our evaluation results.

II. Related Work

Studies have shown that EEG has the potential to be used as a biomarker for various neurological conditions including ASD [8], [9]. It measures the electrical signals of the brain via electrodes placed on various places on the scalp. These electrical signals correspond to postsynaptic activity in the neocortex, and could be used to study complex neuropsychiatric issues. EEG signals have frequency bands that are associated with different activities on the brain. Waves in range $(0, 4)$ Hz belongs to δ frequency band. Likewise, waves in ranges $(4, 7.5)$ Hz, $(7.5, 12)$ Hz, $(12, 30)$ Hz, and $(30, 100)$ Hz belong to θ, α, β and γ frequency bands respectively (see Table II). Studies [10] have shown that having more power on the higher-frequency bands indicate a higher attention, while having more power on the lower-frequency bands indicate otherwise.

Zhao et.al. [11] have used singular spectrum analysis (SSA) to perform feature extraction and classification of EEG signals in autistic children . SSA was proposed to remove artifacts and extract rhythm from EEG signals. They used individualized α peak frequency (PAF) and the relative energy of AFi to create SVM models for classification. Using SSA resulted in an accuracy boost from 81.36% to 89.83%. They also observed an accuracy rate of 94.92% by using relative energies of α rhythm AFi and α peak frequencies as common features. This indicated that abnormal EEG rhythm in autistic children is reflected in two aspects: *frequency distribution* and *power modulation*; the α rhythm of autistic children had a low frequency offset and a decrease in relative energy.

Abdulhay et.al. [12] have used EEG intrinsic function pulsation to identify patterns in Autism. They have mathematically computed EEG features and compared ASD subjects with typically developing (TD) subjects. They have collected resting state EEG from 20 children (10 ASD, 10 non-ASD) using 64 electrodes at a 500 HZ sampling frequency. Raw signals were band pass filtered and ocular artifacts were removed using Independent Component Analysis. Empirical Mode decomposition was applied to extract Intrinsic Mode Functions (IMFs) from each channel. Next, point by point pulsations were computed and plotted for each IMF to compare with IMFs from other channels. Any existing stability loops were analyzed for abnormal neural connectivity. In the first IMF, it was observed that the stability of local pulsation pathways between channel 2 and channel 3 maintained consistency in ASD children while it was random in typically developing children. Similar observations were made in channel pairs (1, 2) and (36, 37). Overall this computational method was able to discover abnormal EEG activities for differentiating between ASD and typically developing children.

Bosl et.al. [9] have formulated a data driven approach to predict ADOS calibrated severity scores and the clinical diagnostic outcome of ASD using EEG measurements collected from 99 infants. Nonlinear features were computed from EEG signals and used as input to statistical learning methods. Through this approach, the authors were able to obtain a highly accurate prediction of ASD, and the ADOS severity scores predicted for all infants in the study were strongly correlated with the actual measured scores. In another study [13], authors have proposed a complex EEG processing algorithm called MSROM/I-FAST along with multiple machine learning algorithms to classify Autistic patients. They used 15 ASD subjects and 10 control subjects to obtain their resting-state EEG readings, which were converted into feature vectors. Multi Scale Entropy (MSE) features and Multi Scale Ranked Organizing Maps (MS-ROM) features were used to train different models. When using MSE features, Logistic Regression and Naive Bayes models have yielded the best results with only two errors. Using MS-ROM have yielded 100% accuracy across all models.

Another study [14] has used Modified Multi Scale Entropy (mMSE) to generate feature vectors and train multi-class SVM models to differentiate between 1) typically developing and 2) high risk infant groups. This categorization was based on having a confirmed ASD diagnosis on an immediate family member. 79 infants (49 high risk infants and 33 typically developing infants) were used for the study, and data was collected from each infant at five sessions spanning a period of 6 to 24 months. In each session, their resting state EEGs were extracted from 64 electrodes by placing the infants in a dimly lit room on their mothers lap and blowing bubbles to grab their attention. The raw signals were preprocessed through mMSE, and their min, max and average entropy values were extracted. The best fit obtained when classifying using these values was at the age of 9 months, with over 90% accuracy.

There have also been research on using EEG for autism severity prediction through empirical mode decomposition and second order difference plots [15]. EEG-based multi-feature fusion assessment approaches to diagnose autism [16] has also been explored. Another study [17] which used machine learning methods to predict of short-term outcomes of ASD concluded that early-age diagnosis and early-start rehabilitation plays a key role in overcoming ASD with time. They also discovered that comorbid psychiatric diagnoses are affecting the outcome of ASD symptoms in clinical observation.

III. Methodology

Based on these findings, we hypothesize that EEG data obtained during the administration of ADOS-2 contains short-term and long-term trends that help to formulate an objective measure for ASD. To validate this hypothesis, a series of pre-processing steps were applied on the raw signals to transform them into a format that contains distinguishable patterns to diagnose ASD. Several feature extraction methods and feature

TABLE I
ADOS-2 SCORES OF EACH SUBJECT [18]

Participant	Sex	Age	ADOS-2	ASD Diagnosis
2	M	10	19	ASD
4	M	17	12	ASD
11	M	6	11	ASD
12	M	16	16	ASD
13	F	11	16	ASD
15	F	10	7	ASD
18	M	5	20	ASD
20	M	15	9	ASD
5	M	11	5	TD
7	F	9	0	TD
8	F	6	5	TD
14	F	16	0	TD
16	M	8	4	TD
17	F	6	0	TD
19	M	15	2	TD
21	M	6	4	TD
22	F	8	0	TD

transformations were employed to generate training and test data that capture these trends. Multiple machine learning models were trained to diagnose ASD and to predict ADOS-2 scores, and were evaluated using standard IR metrics. These metrics were used as the basis to determine the validity of our hypothesis.

A. Participants and ADOS-2 Procedure

We collected bio-behavioral metrics [18] from EEG within the context of standardized tasks used in an assessment of ASD symptomatology: ADOS-2. The ADOS-2 has been carefully developed to create snapshots of naturalistic social scenarios that can reveal observable features central to ASD (e.g., joint attention, gesturing, social overtures), thereby allowing us to measure brain activity that is temporally concurrent with these observable ASD features within relatively brief periods. Thus, we capitalized on the semi-structured and standardized nature of the social tasks of the ADOS-2 to create a context that engaged the social brain system of the participants. Each participant self-identified as having received a positive or diagnosis of ASD by a clinical professional prior to enrolling in this study. 17 individuals (ASD = 8, TD = 9) between the ages of 5 and 17 years (see Table I) were recruited for this study, and asked to complete an ADOS-2 assessment while we simultaneously recorded their EEG. IRB approval was obtained prior to the study, and data was collected in a prospective fashion at IUPUC with informed consent from each participant.

B. EEG Acquisition and Pre-processing

Our preliminary EEG measures were acquired from each subject throughout the administration of ADOS-2, using a 32-channel LiveAmp wireless EEG system with active electrodes and a digital sampling rate of 250 Hz (Brain Products GmbH). All 32 channels were continuously recorded using the FCz electrode as reference. Use of a wireless EEG system allowed for head movements, and the active electrodes increased speed of application, thereby increasing the probability of successful EEG data acquisition with special populations. The raw EEG data was then imported into the open-source MATLAB toolbox, EEGLAB for pre-processing. Figure 1 illustrates the pre-processing pipeline followed to transform the raw signal into a feature-rich format. Additional information about the processing pipeline are available in our previous work [18].

TABLE II
FREQUENCY BANDS USED FOR DECOMPOSITION

Band	Lo (Hz)	Hi (Hz)
δ	0.1	4.0
θ	4.0	7.5
α	7.5	12.0
β	12.0	30.0
γ	30.0	100.0

The resulting signals had a sampling rate of 250 Hz. It had 15,000 samples for the BASELINE epoch, and 45,000 samples each for the START, MIDDLE and END epochs. Figure 2a shows a subset of electrode readings obtained after preprocessing. Each series was named after its corresponding electrode, and contained the full frequency range of the clean signal.

C. Feature Extraction and Analysis

We analyzed the pre-processed signals in two approaches:

- Method 1: Frequency Band Decomposition
- Method 2: Wavelet Transform

Both approaches were evaluated independent of each other using two machine learning models to obtain the results.

1) Frequency Band Decomposition: Signals from each electrode were decomposed into five five signals: δ, θ, α, β and γ, each representing a component of that signal in a frequency band (see Table II). This decomposition was performed using Butterworth filters in the order of 5 (n = 5), whose mathematical equation is given in Equation 1.

$$|H(j\omega)| = 1/\sqrt{1 + \epsilon^2(\omega/\omega_p)^{2n}} \quad (1)$$

Here, ω_p is the cutoff angular velocity, and ϵ is the maximum band pass gain.

Figure 2b shows a subset of the results from this decomposition. Each series represents data within one frequency band of an electrode. For instance, F9_0 represents the δ frequency band of the F9 electrode, and F9_1 represents the θ frequency band of that electrode.

An algorithm was devised to calculate the power matrix for a time series. (see Algorithm 1). Given a set of frequency bands B, a time series S with n samples recorded at a sampling frequency of f, a window size of W seconds and a step size of E seconds, it generates the power matrix by decomposing the signal S into $|B|$ signals corresponding to each band in B, stepping through each decomposed signal in strides of $f \times E$ samples, and calculating the power within a window of $f \times W$ samples. Thus, a $(|B| \times n/(fE))$ matrix

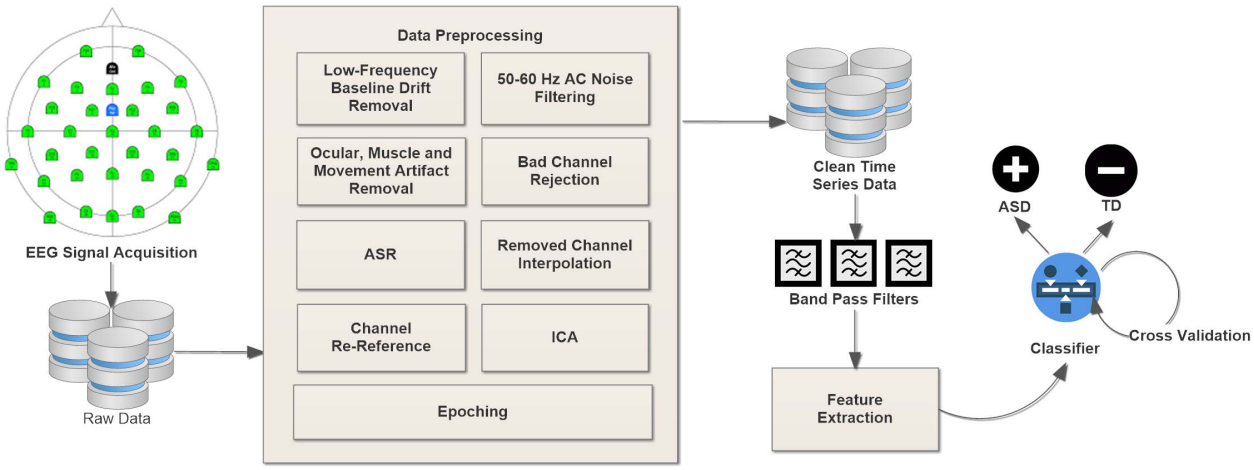

Fig. 1. EEG Processing and Classification Pipeline [18]

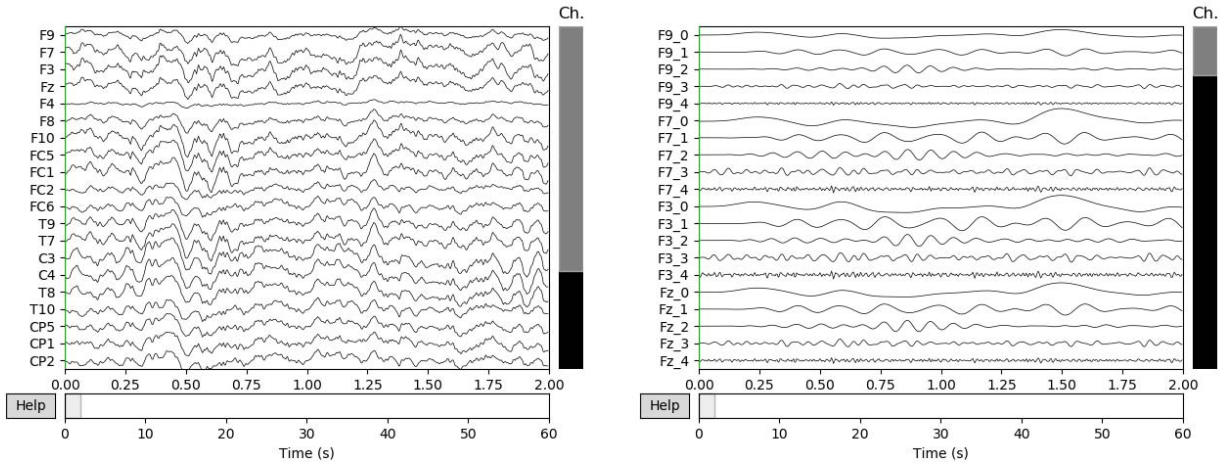

(a) Electrode readings after pre-processing.

(b) Electrode readings after band pass filtering.

Fig. 2. EEG Pre-processing and Band Pass Filtering

was generated for each electrode. The function P used here is described in Equation 2. It calculates the power of a signal S within a window W for a step size E, given the current step j and sampling frequency f.

$$P(S, W, E, j, f) = \frac{1}{W} \sum_{k=0}^{fW-1} |S[Efj + k]|^2 \qquad (2)$$

We initialized the window size and step size to $W = 5$ and $E = 2$ respectively, and generated power matrices for all electrodes of each participant at all epochs.

2) Wavelet Transform: Wavelet transforms were used as an improvement over the former approach to compensate for the loss of resolution when using a fixed-size window to calculate coefficients of the power matrices. The wavelet transform function is described in Equation 3,

$$X(a, b) = \frac{1}{\sqrt{a}} \int_{-\infty}^{+\infty} \psi\left(\frac{t-b}{a}\right) x(t)dt \qquad (3)$$

Here, a and b corresponds to the scale and translation of the wavelet signal ψ, which is convolved over the source signal $x(t)$.

The EEG processing pipeline used in this approach is illustrated in Figure 3. A Complex Morlet Wavelet with a center frequency $f_c = 1Hz$ and a bandwidth of $f_b = 1.5Hz$ (which has been shown to provide a good trade-off between time and frequency localization [19]) was used for this task. We generated wavelet transforms for each signal S at X different scales (X = 150) starting from $1 \times (f/2) = 125Hz$ down to $1 \times (f/2)/150 \approx 0.8Hz$ and generated a $(X \times |S|)$ matrix for each electrode. The resulting matrix was scaled down to $(X \times X)$ using a max aggregator function, to

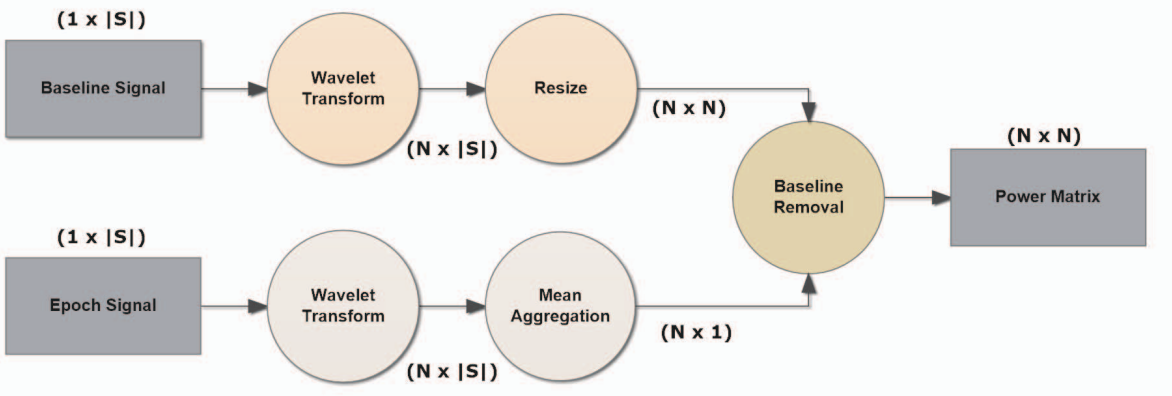

Fig. 3. EEG Processing Pipeline in Wavelet Transform Method

Algorithm 1 Power Matrix of an Electrode

$f \leftarrow sampling\_freq$
function POWERMATRIX(B, S, W, E)
  $F \leftarrow BandPass(B, S)$
  $I \leftarrow |B|$
  $J \leftarrow |S|/(fE)$
  $M \leftarrow array[I][J]$
  for all $i \leftarrow 0, ..(I-1)$ **do**
    for all $j \leftarrow 0, ..(J-1)$ **do**
      $M[i][j] \leftarrow P(F[i], W, E, j, f)$
    end for
  end for
return M
end function

reduce computational complexity. All matrix coefficients were squared to obtain their power equivalent.

Next, each power matrix was referenced to the mean signal strength of the electrode's baseline. When calculating the baseline value for an electrode, a wavelet transform was performed on the BASELINE epoch of that electrode and the resulting matrix was reduced to a column vector using a mean aggregator. This column vector was subtracted from each column of the electrode power matrix to obtain the final matrix.

Figure 4a illustrates the power matrix of a sample electrode for a TD (typically developing) subject. All values were normalized to the (0 - 255) range for illustration purposes. The X axis represents time scaled by a factor of $4x$, and the Y axis represents the scale of the reference wavelet used, which relates to the frequency $f(s)$ as given in Equation 4,

$$f(s) = f_c \times \frac{f}{s} \tag{4}$$

where f_c is the center frequency of the wavelet, f is the sampling frequency, and s is the scale. The color at each (x, y) coordinate corresponds to the signal power at that time and scale. Darker shades represent lower power, while lighter shades represent higher power.

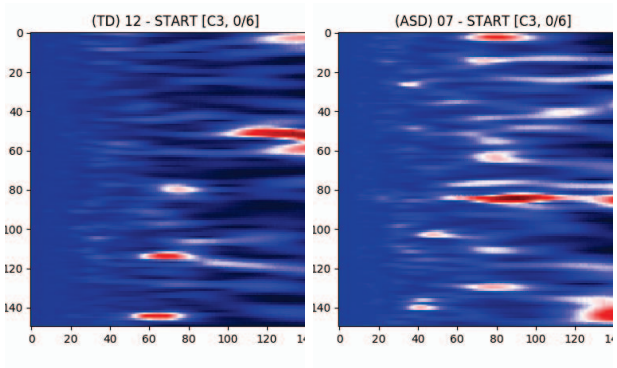

(a) Diagnosis - TD (b) Diagnosis - ASD

Fig. 4. Wavelet Transforms for electrode FC1

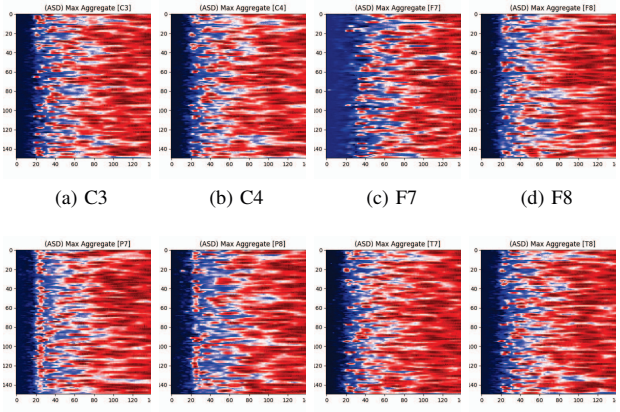

(a) C3 (b) C4 (c) F7 (d) F8

(e) P7 (f) P8 (g) T7 (h) T8

Fig. 5. Aggregate Power Spectrums of all ASD Participants

Figure 4b shows the illustration of a wavelet transform performed on the FC1 electrode, but for an ASD subject. The axes and colors follow the same convention as Figure 4a. Both images are referenced to the mean signal strength of the corresponding electrode as observed in the BASELINE epoch.

Figure 5 provides an illustration for the power spectrums of

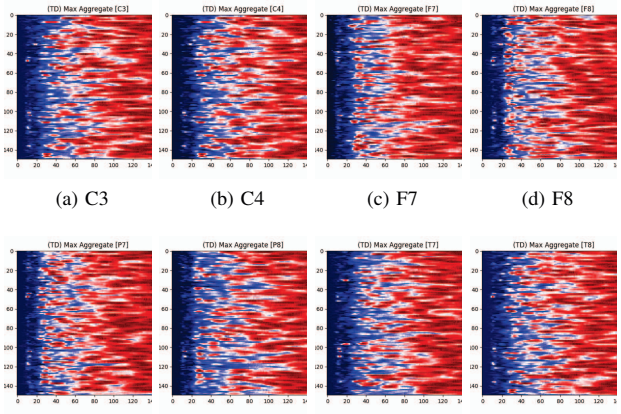

(a) C3 (b) C4 (c) F7 (d) F8

(e) P7 (f) P8 (g) T7 (h) T8

Fig. 6. Aggregate Power Spectrums of all TD Participants

8 EEG electrodes, whose color at each (x, y) coordinate corresponds to the maximum power across all epochs and chunks of all ASD participants for that particular coordinate. A max aggregator function was used to generate this visualization.

Figure 6 shows similar illustrations for the same 8 electrodes given in Figure 5, but with the color at each (x, y) calculated from TD participants instead of ASD participants.

IV. Evaluation and Results

The power matrices obtained through Frequency Band Decomposition and Wavelet Transforms were used to train several machine learning models. We evaluated both short-term and long-term dependencies between ASD and EEG data to determine the nature of their relationship. Our evaluation criteria was based on the following objectives.

- Providing a clinical diagnosis of ASD for each participant (classification)
- Predicting the ADOS-2 score for each participant (regression)

A. Analysis of short-term trends

Here, our goal was to evaluate whether an accurate diagnosis of ASD could be provided without taking long-term trends into account. WEKA [20] was used to perform this analysis, and the evaluation measures were obtained by training models using short-term features: Each power matrix was decomposed into a set of vectors each representing the powers of frequency bands within a window of ($t = 180/150 = 1.2s$). Electrode vectors belonging to that participant, epoch and timestamp were aggregated into a single vector, and treated as one sample. We used these samples to train several models using two approaches: 1) using only Homan et al. [21] electrode placement correlates of cortical locations (F7, F8, T7, T8, TP9, TP10, P7, P8, C3, and C4), and 2) using all electrodes. Precision, recall, accuracy and F1 statistics were obtained for each model and electrode set through 10-fold cross validation.

Tables III and IV show the top performing classifiers (ranked by evaluation statistics) for electrode sets 1 and 2, respectively. It was observed that the RandomForest classifier yielded the highest percent accuracy of 97.04 % for the training samples generated from electrode set 1. The AdaBoostM1 classifier yielded the lowest percent accuracy at 79.75%.

TABLE III
Classification of EEG during ADOS-2 using Homan et al. [21] electrode placement [18]

Classifier	Precision	Recall	F1	Accuracy
Random Forest	0.97	0.97	0.97	**97.04 %**
Logistic	0.84	0.84	0.84	84.72 %
Bagging	0.95	0.95	0.95	**95.50 %**
JRip	0.94	0.94	0.94	94.57 %
LMT	0.83	0.82	0.82	82.94 %
AdaBoostM1	0.80	0.79	0.79	79.75 %

TABLE IV
Classification of EEG during ADOS-2 using all electrode placements [18]

Classifier	Precision	Recall	F1	Accuracy
Random Forest	0.98	0.98	0.98	**97.75 %**
Logistic	0.95	0.95	0.95	94.85 %
Bagging	0.94	0.94	0.94	94.39 %
JRip	0.98	0.98	0.98	**98.27 %**
LMT	0.94	0.94	0.94	93.97 %
AdaBoostM1	0.93	0.92	0.92	92.15 %

Table IV shows the evaluation results when all electrodes were used to generate the training samples. Results show that training samples generated from all electrodes provided a diagnosis for ASD with above 90% accuracy, and had a slight edge over electrode set 1 (98.25% versus 97.04%). Here, JRip yielded the highest percent accuracy of 98.27%, while AdaBoostM1 yielded the lowest at 92.15%.

Table V shows the results of the correlation analysis between the predicted and labelled ADOS-2 Scores. Here, Bagging yielded the highest correlation coefficient (r) of 0.9079, with a Root Mean Squared Error (RMSE) of 2.93. The REP Tree yielded the least correlation coefficient of 0.8174, with a RMSE of 3.87.

B. Analysis of long-term trends

The power matrices were also evaluated using a Convolutional Neural Network (CNN) to account for any temporal relationships in the EEG data. In short-term trend analysis, each column of the power spectrum was taken as an vector regardless of time. But in long-term trend analysis, the power matrix was used as-is. However, unlike in short-term analysis, the power matrices of all electrodes belonging to that participant and epoch were treated as independent samples and not aggregated.

Figure 7 shows the structure of the CNN used for this analysis. The first layer is a 1D Convolution Layer, which uses a kernel of size = 4 to generate (1 x 16) vectors for each convolution. The output of this layer is passed into a Max Pooling Layer which aggregates adjacent vectors using a Max operator. The purpose of this layer is to reduce the resolution of the representation learned by the upper layers to enable

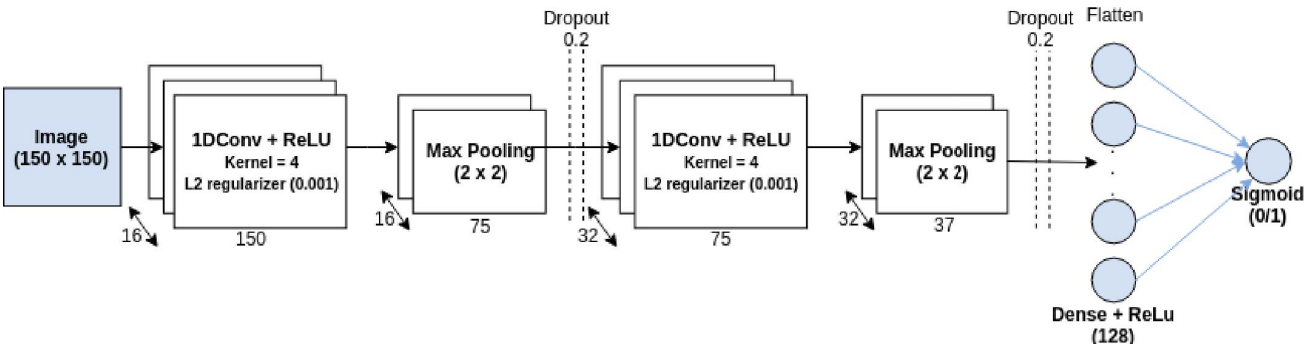

Fig. 7. Layers of the CNN model

TABLE V
CORRELATION ANALYSIS FOR ADOS-2 SCORE

Model	r^2	MAE	RMSE
Random Forest	0.8606	2.2122	**2.9724**
Linear Regression	0.7296	2.7978	3.4921
Bagging	0.8242	1.8986	**2.9342**
REP Tree	0.6681	2.1463	3.8749

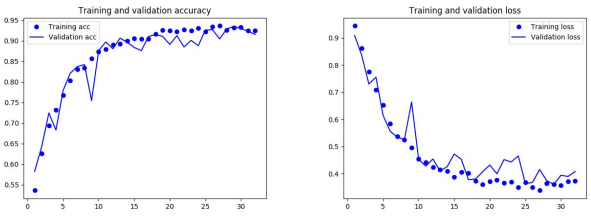

(a) Accuracy (b) Loss

Fig. 8. Training Progress of the CNN Model

lower layers to focus on other details. Next the data passes through a Dropout Layer, which drops 20% of calculated weights to zero to prevent overfitting. The output is then passed on to another 1D Convolution Layer, which uses a kernel of size = 4 to generate (1 x 32) vectors for each convolution. This output is then passed on to another Max Pooling Layer, then to another Dropout Layer, and to a Flatten Layer, which flattens the input matrix into a vector. This output is passed through a Dense Layer, and finally arrives at a Sigmoid Neuron that performs binary classification based on the input from Dense Layer. All Convolution Layers were configured with L2 regularizers to avoid overfitting the data.

A stochastic gradient descent (SGD) optimizer [22] was used for training with a learning rate of 0.01, a decay factor of 10^{-6} and a momentum of 0.9. A $3/1$ split was used for train/test data, and the model was trained for 32 epochs.

Figure 8 illustrates the training progress of the CNN using the given samples, and the respective change in accuracy and loss metrics across each training epoch.

TABLE VI
PERFORMANCE OF SHORT TERM VS LONG TERM CLASSIFIERS

Classifier	Precision	Recall	F1	Accuracy
Random Forest	0.97	0.97	0.97	0.97
CNN	0.95	0.95	0.95	0.95

The classification performance of the CNN model is given in Table VI. Here, it is seen that the both the Random Forest classifier (short-term trends) and CNN (long-term trends) provide a $\geq 95\%$ classification accuracy.

V. DISCUSSION

Results obtained from short-term and long-term trend analysis shows a high correlation of the EEG data with the human-labeled ASD diagnosis and ADOS-2 scores. A slight boost in accuracy by moving from electrode set 1 to electrode set 2 was achieved by adding $32 - 10 = 22$ more electrodes to each training sample. Thus it could be argued that a slight penalty on accuracy is desirable than the added computational complexity from electrode set 2. The best option of the two depends on the requirements and constraints.

One limitation of this study is that it was performed using only 17 participants. As a result, some features such as gender are not balanced between the classes. This could be one reason for observing similar classification powers across short-term and long-term trends. Another reason is that, unlike the models trained for short-term trends, the CNN model was trained with preventive measures against overfitting, such as Dropout Layers and Regularization. Therefore, extending this study by recruiting more subjects could counter these imbalances and provide a more generalized evaluation.

VI. CONCLUSION AND FUTURE OUTLOOK

The notion that EEG during social interaction may be a useful index of social impairment is suggested by both the literature [23], [24] and by our preliminary findings obtained from this study. Despite a small sample size, our preliminary results indicate a trending association between EEG features

and level of social symptom severity (according to the ADOS-2) in children with ASD (see Table I) that is effective enough to provide a clinical diagnosis of ASD, and to predict the ADOS-2 scores with minimal effort and subjectivity. Such diagnostic group differences in association patterns reflect a tendency for children with impaired social capacity to have idiosyncratic patterns of EEG activity relative to typical neuro-development. Our classifiers show utility to predict features in line with diagnostic binary outcome of ASD and TD, and strongly correlates with clinical criteria of ADOS-2. Thus, EEG measures acquired during live social interaction show promise as a candidate non-invasive bio-marker of early emerging aberrant social neuro-cognitive dysfunction in ASD.

In the future we will aim to increase robustness of our classification system by obtaining two sets of bio-behavioral measures: functional integration measures of neuro-cognitive networks associated with the social brain (i.e., EEG coherence) and visual behavior (i.e. eye tracking metrics). With regard to visual behavior, we will collect, analyze, and produce a battery of traditional positional eye movement metrics thought to be potential indicators of joint attention, such as fixations, micro-saccades, and pupil activity during naturalistic, dynamic social communication tasks.

REFERENCES

[1] M. N. Ziats and O. M. Rennert, "The evolving diagnostic and genetic landscapes of autism spectrum disorder," *Frontiers in genetics*, vol. 7, p. 65, 2016.

[2] L. de la Torre-Ubieta, H. Won, J. L. Stein, and D. H. Geschwind, "Advancing the understanding of autism disease mechanisms through genetics," *Nature medicine*, vol. 22, no. 4, p. 345, 2016.

[3] J. Baio, L. Wiggins, D. L. Christensen, M. J. Maenner, J. Daniels, Z. Warren, M. Kurzius-Spencer, W. Zahorodny, C. R. Rosenberg, T. White *et al.*, "Prevalence of autism spectrum disorder among children aged 8 yearsautism and developmental disabilities monitoring network, 11 sites, united states, 2014," *MMWR Surveillance Summaries*, vol. 67, no. 6, p. 1, 2018.

[4] A. V. Buescher, Z. Cidav, M. Knapp, and D. S. Mandell, "Costs of autism spectrum disorders in the united kingdom and the united states," *JAMA pediatrics*, vol. 168, no. 8, pp. 721–728, 2014.

[5] K. Gotham, S. Risi, A. Pickles, and C. Lord, "The autism diagnostic observation schedule: revised algorithms for improved diagnostic validity," *Journal of autism and developmental disorders*, vol. 37, no. 4, p. 613, 2007.

[6] A. Lenartowicz and S. K. Loo, "Use of eeg to diagnose adhd," *Current psychiatry reports*, vol. 16, no. 11, p. 498, 2014.

[7] D. Gloss, J. K. Varma, T. Pringsheim, and M. R. Nuwer, "Practice advisory: The utility of eeg theta/beta power ratio in adhd diagnosis report of the guideline development, dissemination, and implementation subcommittee of the american academy of neurology," *Neurology*, pp. 10–1212, 2016.

[8] J. Wang, J. Barstein, L. E. Ethridge, M. W. Mosconi, Y. Takarae, and J. A. Sweeney, "Resting state eeg abnormalities in autism spectrum disorders," *Journal of neurodevelopmental disorders*, vol. 5, no. 1, p. 24, 2013.

[9] W. J. Bosl, H. Tager-Flusberg, and C. A. Nelson, "Eeg analytics for early detection of autism spectrum disorder: a data-driven approach," *Scientific reports*, vol. 8, no. 1, p. 6828, 2018.

[10] U. Friese, J. Daume, F. Göschl, P. König, P. Wang, and A. K. Engel, "Oscillatory brain activity during multisensory attention reflects activation, disinhibition, and cognitive control," *Scientific reports*, vol. 6, p. 32775, 2016.

[11] J. Zhao, J. Song, H. Chen, X. Li, and J. Kang, "Feature extraction and classification of eeg signals in autistic children based on singular spectrum analysis," *Chinese Science Bulletin*, 2019.

[12] E. Abdulhay, M. Alafeef, H. Hadoush, N. Alomari *et al.*, "Frequency 3d mapping and inter-channel stability of eeg intrinsic function pulsation: Indicators towards autism spectrum diagnosis," in *Electrical and Electronics Engineering Conference (JIEEEC), 2017 10th Jordanian International*. IEEE, 2017, pp. 1–6.

[13] E. Grossi, C. Olivieri, and M. Buscema, "Diagnosis of autism through eeg processed by advanced computational algorithms: A pilot study," *Computer methods and programs in biomedicine*, vol. 142, pp. 73–79, 2017.

[14] W. Bosl, A. Tierney, H. Tager-Flusberg, and C. Nelson, "Eeg complexity as a biomarker for autism spectrum disorder risk," *BMC medicine*, vol. 9, no. 1, p. 18, 2011.

[15] H. Hadoush, M. Alafeef, and E. Abdulhay, "Automated identification for autism severity level: Eeg analysis using empirical mode decomposition and second order difference plot," *Behavioural brain research*, vol. 362, pp. 240–248, 2019.

[16] J. Kang, T. Zhou, J. Han, and X. Li, "Eeg-based multi-feature fusion assessment for autism," *Journal of Clinical Neuroscience*, vol. 56, pp. 101–107, 2018.

[17] M. B. Usta, K. Karabekiroglu, B. Sahin, M. Aydin, A. Bozkurt, T. Karaosman, A. Aral, C. Cobanoglu, A. D. Kurt, N. Kesim *et al.*, "Use of machine learning methods in prediction of short-term outcome in autism spectrum disorders," *Psychiatry and Clinical Psychopharmacology*, pp. 1–6, 2018.

[18] S. Jayarathna, Y. Jayawardana, M. Jaime, and S. Thapaliya, "Electroencephalogram (EEG) for Delineating Objective Measure of Autism Spectrum Disorder," in *Computational Models for Biomedical Reasoning and Problem Solving*, C. S.-C. Chen, Chung-Hao, Ed. IGI Global, 2019.

[19] K. Müller, G. Lohmann, J. Neumann, M. Grigutsch, T. Mildner, and D. Y. von Cramon, "Investigating the wavelet coherence phase of the bold signal," *Journal of Magnetic Resonance Imaging: An Official Journal of the International Society for Magnetic Resonance in Medicine*, vol. 20, no. 1, pp. 145–152, 2004.

[20] Z. Markov and I. Russell, "An introduction to the weka data mining system," *ACM SIGCSE Bulletin*, vol. 38, no. 3, pp. 367–368, 2006.

[21] R. W. Homan, J. Herman, and P. Purdy, "Cerebral location of international 10–20 system electrode placement," *Electroencephalography and clinical neurophysiology*, vol. 66, no. 4, pp. 376–382, 1987.

[22] L. Bottou, "Large-scale machine learning with stochastic gradient descent," in *Proceedings of COMPSTAT'2010*. Springer, 2010, pp. 177–186.

[23] P. C. Mundy, *Autism and joint attention: Development, neuroscience, and clinical fundamentals*. Guilford Publications, 2016.

[24] M. Jaime, C. M. McMahon, B. C. Davidson, L. C. Newell, P. C. Mundy, and H. A. Henderson, "Brief report: reduced temporal-central eeg alpha coherence during joint attention perception in adolescents with autism spectrum disorder," *Journal of autism and developmental disorders*, vol. 46, no. 4, pp. 1477–1489, 2016.